ACS APPLIED MATERIALS & INTERFACES

Research Article

www.acsami.org

Tunable Electrical Conductivity and Magnetic Property of the Two Dimensional Metal Organic Framework [Cu(TPyP)$Cu_2(O_2CCH_3)_4$]

Ananya Sengupta,[†,‡] Subhadeep Datta,[†,‡] Chenliang Su,[†] Tun Seng Herng,[§] Jun Ding,[§] Jagadese J. Vittal,[*,‡] and Kian Ping Loh[*,‡,∥]

[†]SZU-NUS Collaborative Innovation Center for Optoelectronic Science & Technology and Key Laboratory of Optoelectronic Devices and Systems of Ministry of Education, College of Optoelectronic Engineering, Shenzhen University, Shenzhen 518060, China

[‡]Department of Chemistry, National University of Singapore, 3 Science Drive 3, Singapore 117543, Singapore

[§]Department of Materials Science & Engineering, National University of Singapore, Singapore 119260, Singapore

[∥]Centre for Advanced 2D Materials (CA2DM) and Graphene Research Centre, National University of Singapore, 6 Science Drive 2, Singapore 117546, Singapore

Supporting Information

ABSTRACT: The coordination chemistry between copper acetate [$Cu_2(OAc)_4$] and 5,10,15,20-tetra-4-pyridyl-21*H*,23*H*-porphine (porphyrin, H_2TPyP) is found to give rise to either a 2D metal−organic framework (MOF) [Cu(TPyP)-$Cu_2(O_2CCH_3)_4$] or a 3D MOF [Cu(TPyP)$CuCl_2$]·2.5TCE·$7H_2O$], depending on the choice of solvent. The 2D MOF can be made into a film, which was doped with 7,7,8,8-tetracyanoquinodimethane (TCNQ), and the electrical conductivity of the thin film was increased by 3 orders of magnitude with respect to that of the undoped Cu-MOF. The formation of a charge-transfer complex between TCNQ and the 2D Cu-MOF also imparts stronger paramagnetic properties than for the undoped MOF.

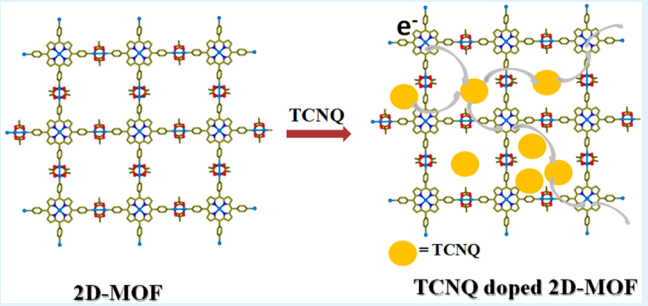

KEYWORDS: *coordination chemistry, metal−organic framework, doping, charge-transfer complex, thin film, conductivity*

INTRODUCTION

A metal−organic framework (MOF) is a highly ordered array of coordination compounds extending through exodentate spacer ligands. These framework structures with well-ordered pores are unique materials for applications in gas storage, gas separation, sensing, and catalysis.[1−3] MOFs are typically poor electrical conductors[4] because of the poor overlap between the d orbitals of the metals and π orbital of the insulating organic ligands.[5,6] For example, a two-dimensional layered MOF, such as iron(II) pyrimidine-2 thiolate, is an insulator.[7] However, an increasing number of proton-conducting MOFs have been reported in the past few years.[8−10] In the case of proton-conducting MOFs, the hydrogen-bonding network, which is created by adsorbed water and numerous dangling groups on the surface of the MOF nanosheets, acts as the pathway for proton transport. Hydroxide ion conduction in MOF has been reported recently.[11] A few examples of conducting MOFs had been prepared with iodine doping.[12−14] The construction of MOFs using new strategies to tune both porosity and electrical conductivity has received interest in the last 5 years.[4] For example, metal triazolate MOFs were found to exhibit ohmic conductivity.[15] Moreover, Dincă and co-workers showed that the bulk electrical conductivity values of both Fe_2(DSBDC) ($DSBDC^{4-}$ = 2,5- disulfhydrylbenzene-1,4-dicarboxylate) and Fe_2(DOBDC) ($DOBDC^{4-}$ = 2,5-dihydroxybenzene-1,4-dicarboxylate) are ∼6 orders of magnitude higher than those of the Mn^{2+} analogues. Fe_2(DSBDC) and Fe_2(DOBDC) exhibit conductivities of 3.9×10^{-6} and 3.2×10^{-7} S/cm, respectively.[16] A nickel-based metal−organic graphene analogue has also been reported with good electrical conductivity of 2 and 40 S/cm for bulk (pellet) and surface (film), respectively.[17] Talin et al. reported a doped metal−organic framework with a good conductivity of 7 S/m.[18] Ab initio calculations suggested a possible mechanism for the conductance in hybrids. The calculations predict that dopant binds strongly to the MOF and creates a continuous path through the unit cell. Recently, silver-nanocluster-doped MOF showed conductivities of 1.8×10^{-8} S/cm under light irradiation.[19] However, 2D MOF exfoliation and thin film device of 2D MOF is rarely reported in literature.[17]

Here we have prepared 2D and 3D MOFs with the organic ligand porphyrin (H_2TPyP) and copper acetate as the starting materials. Porphyrin is chosen due to its electron-accepting property (p-type). Employing the specific host−guest chemistry[20] and high surface area of MOFs, we have successfully doped the 2D MOF with 7,7,8,8-tetracyanoquinodimethane (TCNQ) and improved its electrical and magnetic properties.

Received: March 11, 2016
Accepted: June 6, 2016
Published: June 6, 2016

DOI: 10.1021/acsami.6b03073
ACS Appl. Mater. Interfaces 2016, 8, 16154−16159

RESULTS AND DISCUSSION

When 5,10,15,20-tetra-4-pyridyl-21*H*,23*H*-porphine (H_2TPyP) was reacted with dicopper(II) tetraacetate [$Cu_2(OAc)_4$] by the layering method, an unexpected 3D MOF was obtained. Chlorine from the tetrachloroethane[21,22] (TCE) has been incorporated into the MOF, rendering [$Cu(TPyP)CuCl_2$]·2.5TCE·7H_2O (**1**). The red, blocklike crystals of **1** crystallized in the tetragonal space group $P4_22_12$ (No. 94) with $Z = 4$. The asymmetric unit contains only one-fourth of the formula unit due to different crystallographic symmetries present in this structure. The four pyridyl groups of the ligand are bonded to four "$CuCl_2$" units, so Cu2 has a distorted octahedral coordination geometry with a $CuCl_2N_4$ core as opposed to the Cu1 atom occupying the center of the ligand [see the Supporting Information (SI), Figure S1a]. The pyridyl nitrogen atoms form a square node, and nitrogen atoms of the octahedral Cu2 also form another square node. These squares are nicely translated along the [$\bar{1}10$] axis, but due to streric hindrance, they were twisted by 90° along the *c*-axis, as shown in the SI (Figure S1b). This connectivity yields a three-dimensional network structure (SI, Figure S1c) with the well-known **cds** topology.[23] The 3D structure is non-interpenetrated due to bulky panels. The total potential solvent area volume as calculated by PLATON[24,25] is 2303.5 Å^3 without the guest solvents, which is 63.6% of the unit cell volume of 3619.7(5) Å^3. The calculated density of the crystal without the guest solvents is 0.747 g cm^{-3}. The refinement of as-synthesized 3D MOF (Figure S3), FT-IR spectra (Figure S4), and EPR spectra (Figure S5) are shown in the SI. The pores of **1** are filled with guest solvent molecules, which can be exchanged with MeOH. Moreover, the structure retains its crystallinity after removal of all the guest solvents, as confirmed by powder X-ray diffraction pattern (PXRD) (SI, Figure S2).

When the solvent was changed from tetrachloroethane to chloroform and H_2TPyP was mixed with dicopper(II) tetraacetate, a 2D Cu-MOF, [$Cu_2(OAc)_4(CuTPyP)_{1/2}$]·$CHCl_3$ (**2**) was obtained. The structure of the bulk powder was confirmed by comparing its PXRD patterns with that simulated from the single crystal data.[26] In **2**, all four pyridyl groups of CuTPyP are coordinated to four different Cu(II) atoms of $Cu_2(OAc)_4$ units, resulting in an undistorted 22.2 Å square-grid network. The 2D layers stack in an "*abab*..." sequence, and the networks do not penetrate with each other. The 2D layers stacked along the *c* axis, which has an interlayer separation of $^1/_2c$ (ca. 7.12 Å). The layered compound **2** shows a weight loss of 7.2%, correspond to the loss of 0.05 chloroform and 0.5 water molecules (calculated, 7.1%) in the temperature range 45−150 °C in the thermogravimetric analysis (TGA). Then a second weight loss at 150−315 °C during TGA is due to the decomposition of the framework (SI, Figure S6). Interestingly, **1** was obtained by the layering method with long reaction time and slow diffusion rate, whereas **2** was formed by instant synthesis (Figure 1). Therefore, the crucial point for 3D structure formation is the formation of $CuCl_2$ from the dicopper tetraacetate by the layering method.

We discovered that 2D-MOF (**2**) can be doped without altering its crystal structure. Redox active, electron-accepting TCNQ was utilized to dope **2**. Crystals of **2** were soaked in a saturated solution of TCNQ at room temperature and the

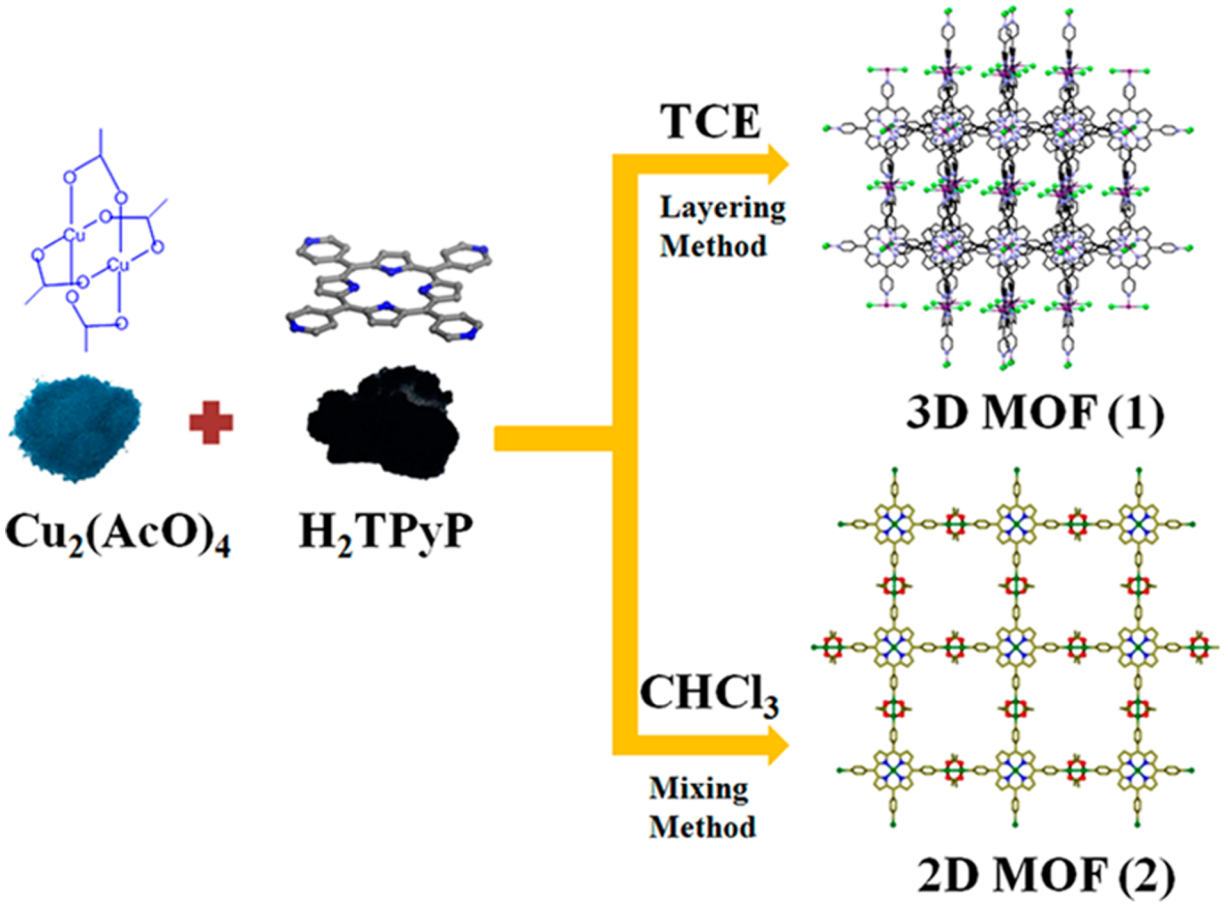

Figure 1. Schematic representation of the preparation of the Cu−porphyrin MOFs **1** and **2**.

DOI: 10.1021/acsami.6b03073
ACS Appl. Mater. Interfaces 2016, 8, 16154−16159

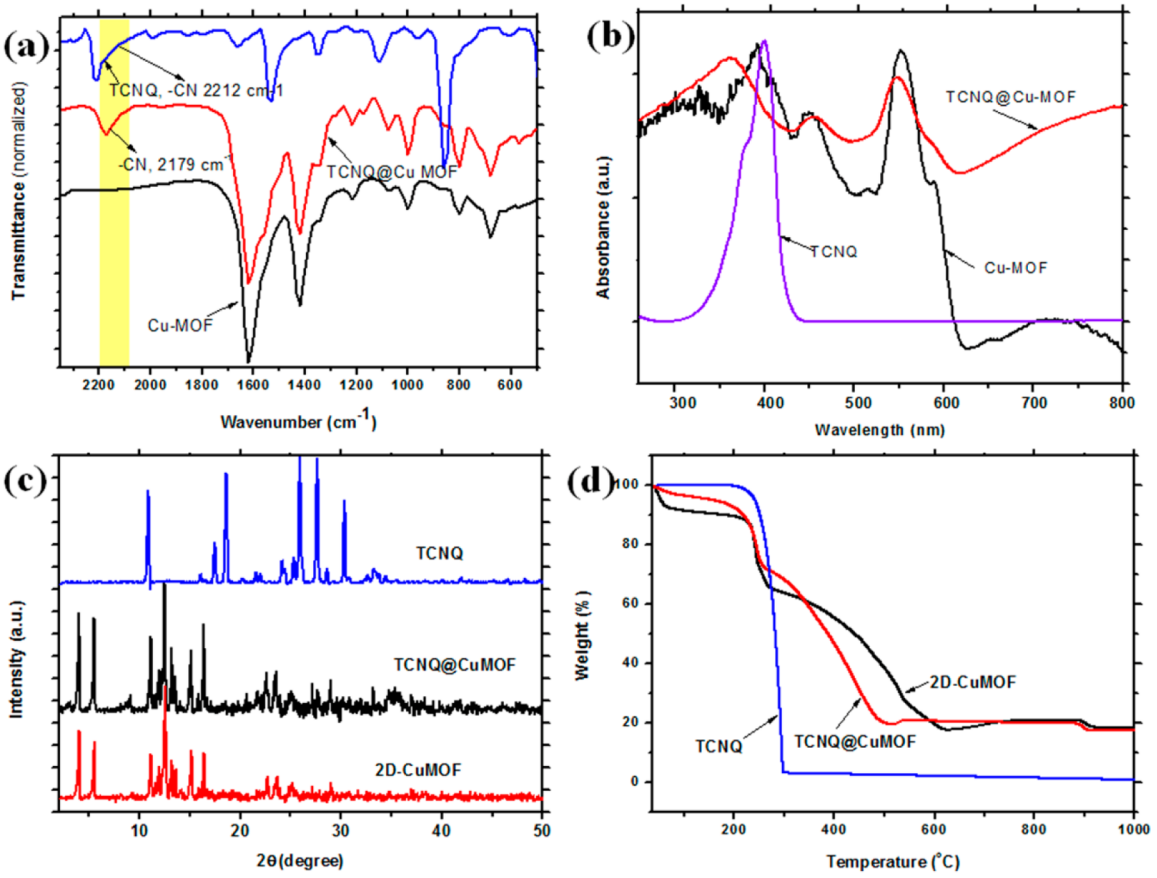

Figure 2. (a) Normalized FT-IR spectra of **2** (black), **3** (red), and TCNQ (blue). (b) Solid-state UV absorption spectra of **2** (black), **3** (red), and TCNQ in dichloromethane (violet). (c) PXRD of **2** (red), **3** (black), and TCNQ (blue). (d) TGA curves of **2** (black), **3** (red), and TCNQ (blue).

guest molecules in **2** were exchanged with the conductive TCNQ molecule. The TCNQ doping was monitored by Fourier transform infrared (FTIR) spectroscopy (Figure 2a), where the −CN stretching frequency appeared at 2179 cm^{-1}, whereas the −CN stretching peak of TCNQ normally appears at 2210 cm^{-1}. The PXRD (Figure 2c) patterns of **2** and TCNQ-doped **2** (**3**) showed that the crystalline structure of **2** was unaltered by the doping process. Solid-state ultraviolet−visible (UV) spectra (Figure 2b) were collected from **2** and TCNQ-doped **2** (**3**). The absorption spectrum of TCNQ-doped Cu-MOF showed a clear blue shift for the porphyrin vibration peak at 353 and a new, broad absorption band at ∼700−800 nm, which originates from the formation of a charge-transfer[27] complex between TCNQ and metalloporphyrin MOF. Moreover, visual inspection of the powdered MOFs revealed that the red color of the parent MOF changed to blackish red after exposure to TCNQ solution (SI, Figure S8). The color of the TCNQ-doped MOF (**3**) did not change upon exposure to air, and it is stable at room temperature for a long time (SI, Figure S9). We note that copper acetate and TCNQ in methanol produces no precipitates; thus, the charge-transfer composite is due entirely to Cu-MOF. As shown in the TGA profile (Figure 2d), sample **2** loses guest solvent molecules upon heating, while the **3** is more stable because the solvent molecules are replaced by TCNQ. Electron paramagnetic resonance (EPR) (SI, Figure S10) of the solid materials provides evidence of the doping. A weak signal of **2** confirms the presence of an unpaired electron in **2**, corresponding to the d^9 system for Cu(II). The paramagnetic intensity increased after TCNQ doping, clearly indicating the formation of TCNQ radical anion.

Preparation of MOFs in the form of bulk powder is well-developed, although there is lack of a procedure for growing thin film of 2D MOFs on surfaces.[28,29] The nanosheets of $[Cu(TPyP)Cu_2(O_2CCH_3)_4]$ (**2**) were synthesized by using an aqueous solution of copper acetate (upper layer) and a chloroform solution of ligand (lower layer). Room temperature reaction led to the generation of a thin film at the water−chloroform interface, which was transferred from the interface onto the substrate. The as-prepared thin film was not soluble in either water or any organic solvent due to the polymeric nature of the **2**. The optical and SEM images (Figure 3a) of the film

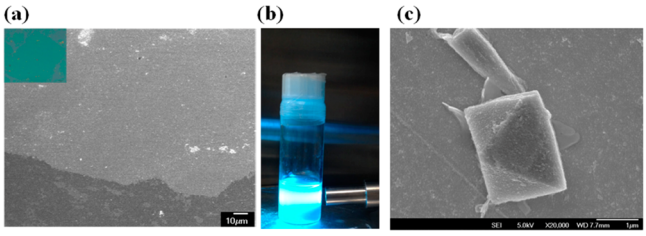

Figure 3. (a) Optical (inset) and scanning electron microscopic (SEM) images of the 2D MOF film (scale bar 10 μm). (b) The Tyndall effect of colloidal 2D MOF (scattering of light) in ethanol. (c) SEM image of exfoliated 2D MOF nanosheets (scale bar 1 μm).

indicate that it has a flat and uniform morphology. Atomic force microscopy (AFM) shows that the average thickness of the 2D MOF film is around 70 nm (SI, Figure S13). Generally, synthesis of MOFs in the form of nanosheets or nanofilms is

DOI: 10.1021/acsami.6b03073
ACS Appl. Mater. Interfaces 2016, 8, 16154−16159

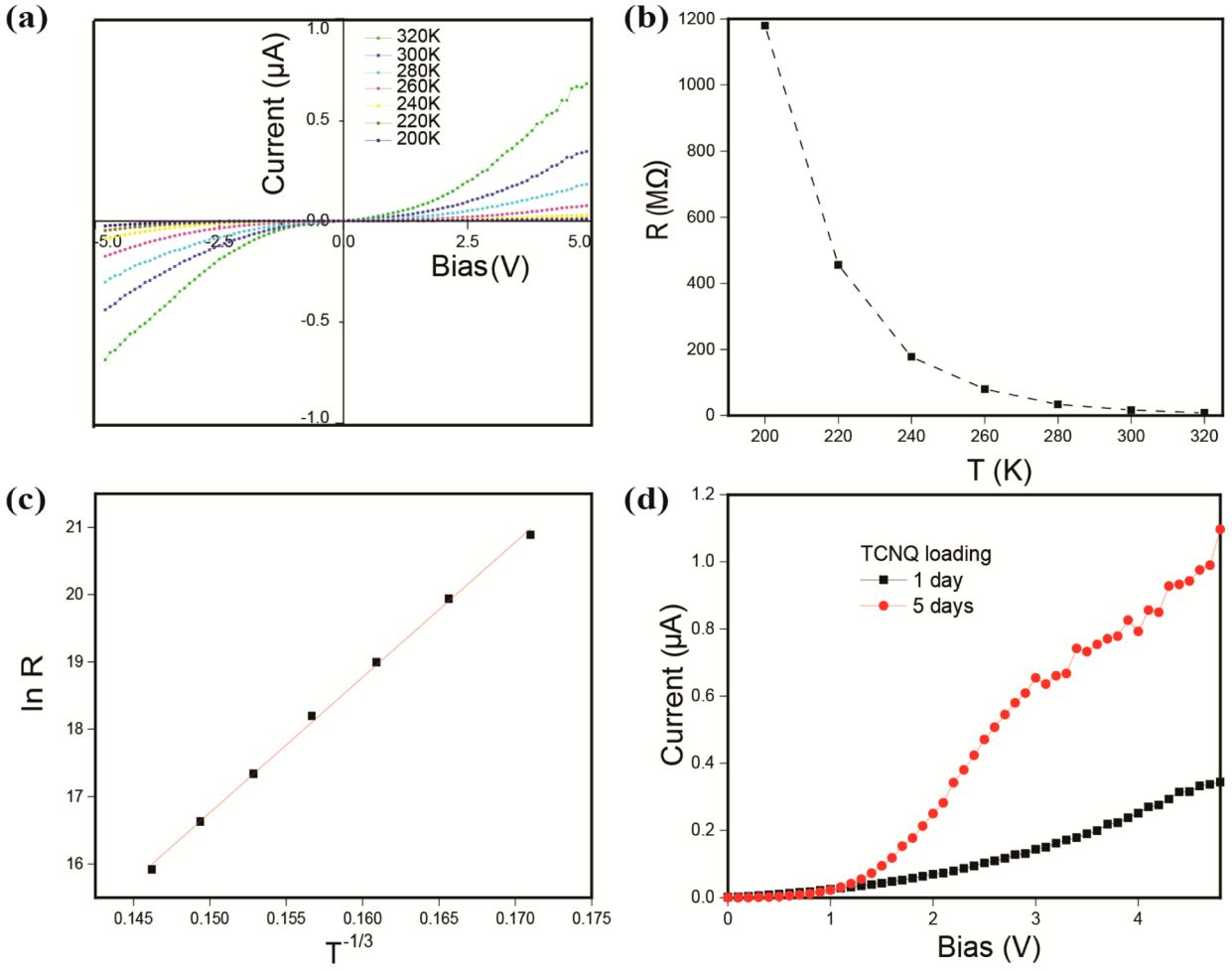

Figure 4. (a) Temperature-dependent $I-V$ curve of the TCNQ-doped 2D MOF film **2**. (b) Temperature-dependent resistance of the device as extracted from the slope of the linear fit of the high bias region of 4a for each temperature plot. (c) Mott variable-range hopping fit of ln R vs $T^{-1/3}$ plot for $d = 2$. (d) $I-V$ curve of the TCNQ-doped 2D MOF film after dipping in a solution of TCNQ for 1 and 5 days.

challenging.[30,31] The 2D MOF could be exfoliated in ethanol by sonication and the exfoliated sheet has an average lateral size of 1.6 ± 0.4 μm (Figure 3c) and an average thickness of 5 nm (SI, Figure S15). The Tyndall effect was observed in the ethanolic solution of 2D MOF, which confirmed the thin and colloidal nature of the exfoliated sheets (Figure 3b).

The 2D MOF film for electrical measurement was grown on a silicon wafer. A very dilute solution of copper acetate and ligand (H_2TPyP) in chloroform and methanol were mixed at room temperature to initiate the nucleation, and then a piece of silicon that had been previously contacted with Ti/Au gold electrodes was immersed into the solution for 24 h at room temperature. The assembled MOF film is homogeneous and dense.

The conductivity measurements were carried out in a physical property measurement system (PPMS, Quantum Design) equipped with a Keithley 6430 sub-femtoamp programmable source meter. Room temperature $I-V$ measurement of the as-grown 2D MOF film conducted in vacuum exhibited very low conductivity (~10^{-7} S/m), which is consistent with its insulating nature. After doping with TCNQ, room temperature conductivity increases to 1×10^{-4} S/m (0.1 μS/mm), 3 orders of magnitude higher than that of the undoped samples. The $I-V$ curves are nonlinear at all temperatures (Figure 4a) and show no hysteresis at the ramp rates used (~100 mV/s). A typical value of two terminal resistances (R), calculated from the slope of the linear part of $I-V$ curve, is 2.5×10^{-4} S/m (0.25 μS/mm) at 320 K. The resistance shows a monotonic increase (Figure 4b) as the temperature decreases, and the $I-V$ curves are highly asymmetric below 240 K. At higher temperature, voltage thresholds (around 200 mV at room temperature) appear above which nonlinearity is evident. Mott's variable-range hopping (M-VRH) (Figure 5a) can be used to explain the temperature dependence of the $I-V$ curves. According to this theory, conduction between localized states near Fermi level EF is governed by hopping of localized electrons and the resistance R of d- dimensional sample as a function of temperature T is given by

$$R = R_0 e^{(T_0/T)^{1/(d+1)}}$$

In our case, logarithmic resistance R (Figure 4c) follows very well the $d = 2$ M-VRH law, which is consistent with the two-dimensional nature of the MOF. The origin of the electronic coupling between TCNQ-doped 2D MOF hybrid complexes is the insertion of the unoccupied molecular orbital of TCNQ in the HOMO−LUMO gap of the MOF. Due to the global structural order, electrons could hop from one localized site to another when receiving energy from an external electrical field.

Such hopping is only possible when TCNQ is inserted into the pore of the MOF framework and provides a conductive channel through the unit cell of **2**. Moreover, the conductivity of the TCNQ-doped MOF (**3**) is increased at least 3 times (3×10^{-4} S/m)

DOI: 10.1021/acsami.6b03073
ACS Appl. Mater. Interfaces 2016, 8, 16154−16159

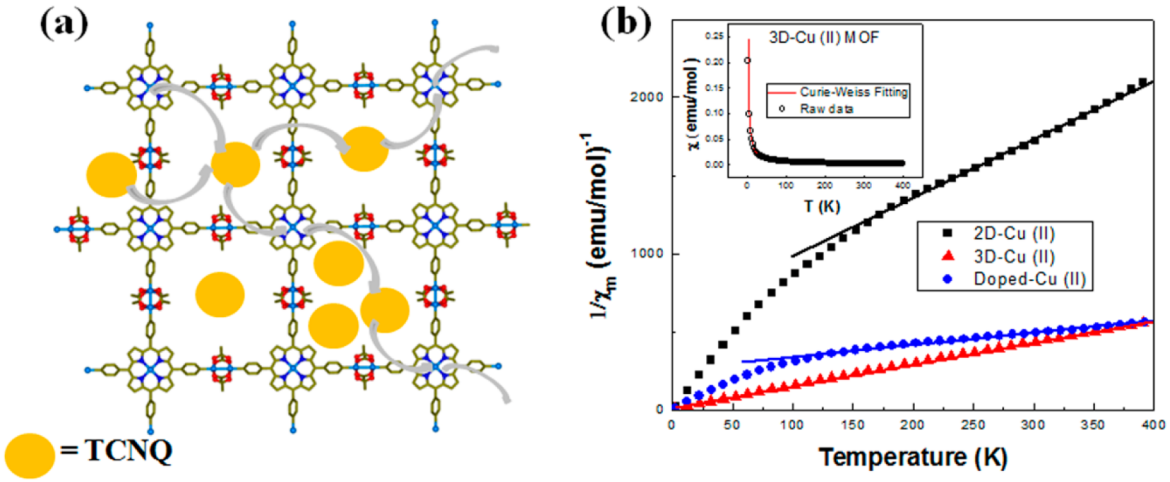

Figure 5. (a) Schematic diagram of the electron-sharing TCNQ molecules in the metalloporphyrin framework. The arrows illustrate the electron-hopping mechanism, which gives rise to electrical conductivity in these material. (b) The $1/\chi_M$ versus T plot of TCNQ-doped 2D MOF (blue), undoped 2D MOF (black), and 3D MOF (red). The raw data of χ_M agrees well with Curie−Weiss fitting.

after dipping it in the TCNQ solution for 5 days (Figure 4d), which reflects that the conductivity is related to the loading concentration of TCNQ in **2**. We find that it is not easy to process the 3D MOF in the form of a thin film, in contrast to the 2D MOF;, therefore, only 2D MOF was chosen for conductivity measurement.

Copper-based MOFs [Cu(II), d^9] with dinuclear Cu(II) are well-known to undergo magnetic superexchange interactions between copper atoms through the bridging ligands. The distance between the copper metal centers and the type of bridging ligand have vital impacts on the magnetic property of copper-based MOFs. Moreover, TCNQ-doped Cu-MOF (**3**) produces charge-transfer complexes that consist of electron donors and acceptors.

The χ_M^{-1} versus T plots of **1**−**3** shown in Figure 5b were characterized by a superconducting quantum interference device (SQUID) magnetometer. Due to the presence of unpaired spin, **1** exhibits paramagnetic properties, with the highest magnetic moment among the three samples in the range from 2 to 400 K. The value of effective magnetic moment per molecule (μ_{eff}) is 1.73 μB, a typical value of a single uncoupled copper ion[32] (1.73 μB, g = 2). The Curie constant of **1** is 0.557 emu K mol^{-1} and the measured data agrees well with Curie−Weiss fitting, as illustrated in the inset of Figure 5b.

For TCNQ-doped 2D MOF and pristine 2D MOF, the χ_M product gradually increases with temperature. The χ_M product of the doped 2D MOF increases from 42.2 (emu $mol)^{-1}$ at 10 K to 555.8 (emu $mol)^{-1}$ at 400 K. The corresponding effective magnetic moment per molecule (μ_{eff}) of doped 2D MOF at 300 K is 1.103 μB, which is higher than the μ_{eff} = 0.59 μB of undoped 2D MOF at 300 K. The increment of the μ_{eff} value for the TCNQ-doped 2D MOF is due to the presence of the carbon radical generated in the charge-transfer complex formed between TCNQ and 2D MOF (**2**). The 2D MOF possesses a Weiss constant of −160 K and Curie constant of 0.0767 emu K mol^{-1}. It is noted that the effective magnetic moments of undoped 2D MOF and doped 2D MOF are smaller than that of single uncoupled Cu(II) ion, which is due to the antiferromagnetic interactions of the two Cu centers within the paddle-wheel cluster.[33,34] This is because the unpaired electron density from both copper ions is transferred to the same orbital of the bridging ligand.

CONCLUSIONS

In summary, we showed that coordination chemistry between $Cu_2(OAc)_4$ and porphyrin (H_2TPyP) can produce two structurally distinct Cu-MOFs, **1** and **2**, which have 3D and 2D structures, respectively. A water−chloroform interfacial synthesis between H_2TPyP and copper acetate produces the 2D Cu-MOF as multilayer nanosheets at the chloroform−water interface. Doping the 2D MOF with TCNQ to form a charge-transfer complex improves its electrical conductivity by orders of magnitude and also improves its magnetic moment. Our work suggests that changing the solvents during the synthesis of MOF may allow 2D MOF to be synthesized from coordination chemistry designed for 3D MOF, opening up fascinating possibilities for 2D films with novel properties.

ASSOCIATED CONTENT

Supporting Information

The Supporting Information is available free of charge on the ACS Publications website at DOI: 10.1021/acsami.6b03073.

Experimental details, crystal structure model, FT-IR, PXRD, EPR, TGA, AFM, and SEM images (PDF)

Crystallographic data for **1** in CIF format (CCDC no. 1454129) (CIF)

AUTHOR INFORMATION

Corresponding Authors

*J.J.V. e-mail: chmjjv@nus.edu.sg.

*K.P.L. e-mail: chmlohkp@nus.edu.sg

Notes

The authors declare no competing financial interest.

ACKNOWLEDGMENTS

The authors like to acknowledge funding support from MOE2014-T3-1-004.

REFERENCES

(1) Long, J. R.; Yaghi, O. M. The Pervasive Chemistry of Metal-Organic Frameworks. *Chem. Soc. Rev.* **2009**, *38*, 1213−1214.

(2) Li, J.-R.; Kuppler, R. J.; Zhou, H.-C. Selective Gas Adsorption and Separation in Metal-Organic Frameworks. *Chem. Soc. Rev.* **2009**, *38*, 1477−1504.

DOI: 10.1021/acsami.6b03073
ACS Appl. Mater. Interfaces 2016, 8, 16154−16159

(3) Zhou, H.-C.; Long, J. R.; Yaghi, O. M. Introduction to Metal−Organic Frameworks. *Chem. Rev.* **2012**, *112*, 673−674.
(4) Sun, L.; Campbell, M. G.; Dincă, M. Electrically Conductive Porous Metal−Organic Frameworks. *Angew. Chem., Int. Ed.* **2016**, *55*, 3566−3579.
(5) Zhu, Q.-L.; Xu, Q. Metal-Organic Framework Composites. *Chem. Soc. Rev.* **2014**, *43*, 5468−5512.
(6) Meek, S. T.; Greathouse, J. A.; Allendorf, M. D. Metal-Organic Frameworks: A Rapidly Growing Class of Versatile Nanoporous Materials. *Adv. Mater.* **2011**, *23*, 249−267.
(7) Beldon, P. J.; Tominaka, S.; Singh, P.; Saha Dasgupta, T.; Bithell, E. G.; Cheetham, A. K. Layered Structures and Nanosheets of Pyrimidinethiolate Coordination Polymers. *Chem. Commun.* **2014**, *50*, 3955−3957.
(8) Xu, G.; Otsubo, K.; Yamada, T.; Sakaida, S.; Kitagawa, H. Superprotonic Conductivity in a Highly Oriented Crystalline Metal-Organic Framework Nanofilm. *J. Am. Chem. Soc.* **2013**, *135*, 7438−7441.
(9) Nagarkar, S. S.; Unni, S. M.; Sharma, A.; Kurungot, S.; Ghosh, S. K. Two-in-One: Inherent Anhydrous and Water-Assisted High Proton Conduction in a 3d Metal-Organic Framework. *Angew. Chem., Int. Ed.* **2014**, *53*, 2638−2642.
(10) Hurd, J. A.; Vaidhyanathan, R.; Thangadurai, V.; Ratcliffe, C. I.; Moudrakovski, I. L.; Shimizu, G. K. H. Anhydrous Proton Conduction at 150 °C in a Crystalline Metal-Organic Framework. *Nat. Chem.* **2009**, *1*, 705−710.
(11) Sadakiyo, M.; Kasai, H.; Kato, K.; Takata, M.; Yamauchi, M. Design and Synthesis of Hydroxide Ion-Conductive Metal-Organic Frameworks Based on Salt Inclusion. *J. Am. Chem. Soc.* **2014**, *136*, 1702−1705.
(12) Zeng, M.-H.; Wang, Q.-X.; Tan, Y.-X.; Hu, S.; Zhao, H.-X.; Long, L.-S.; Kurmoo, M. Rigid Pillars and Double Walls in a Porous Metal-Organic Framework: Single-Crystal to Single-Crystal, Controlled Uptake and Release of Iodine and Electrical Conductivity. *J. Am. Chem. Soc.* **2010**, *132*, 2561−2563.
(13) Kobayashi, Y.; Jacobs, B.; Allendorf, M. D.; Long, J. R. Conductivity, Doping, and Redox Chemistry of a Microporous Dithiolene-Based Metal-Organic Framework. *Chem. Mater.* **2010**, *22*, 4120−4122.
(14) Lu, C.; Ben, T.; Xu, S.; Qiu, S. Electrochemical Synthesis of a Microporous Conductive Polymer Based on a Metal-Organic Framework Thin Film. *Angew. Chem., Int. Ed.* **2014**, *53*, 6454−6458.
(15) Gándara, F.; Uribe-Romo, F. J.; Britt, D. K.; Furukawa, H.; Lei, L.; Cheng, R.; Duan, X.; O'Keeffe, M.; Yaghi, O. M. Porous, Conductive Metal-Triazolates and Their Structural Elucidation by the Charge-Flipping Method. *Chem. - Eur. J.* **2012**, *18*, 10595−10601.
(16) Sun, L.; Hendon, C. H.; Minier, M. A.; Walsh, A.; Dincă, M. Million-Fold Electrical Conductivity Enhancement in Fe2(Debdc) Versus Mn2(Debdc) (E = S, O). *J. Am. Chem. Soc.* **2015**, *137*, 6164−6167.
(17) Sheberla, D.; Sun, L.; Blood-Forsythe, M. A.; Er, S.; Wade, C. R.; Brozek, C. K.; Aspuru-Guzik, A.; Dincă, M. High Electrical Conductivity in Ni3(2,3,6,7,10,11-Hexaiminotriphenylene)2, a Semiconducting Metal−Organic Graphene Analogue. *J. Am. Chem. Soc.* **2014**, *136*, 8859−8862.
(18) Talin, A. A.; Centrone, A.; Ford, A. C.; Foster, M. E.; Stavila, V.; Haney, P.; Kinney, R. A.; Szalai, V.; El Gabaly, F.; Yoon, H. P.; Leonard, F.; Allendorf, M. D. Tunable Electrical Conductivity in Metal-Organic Framework Thin-Film Devices. *Science* **2014**, *343*, 66−69.
(19) Han, S.; Warren, S. C.; Yoon, S. M.; Malliakas, C. D.; Hou, X.; Wei, Y.; Kanatzidis, M. G.; Grzybowski, B. A. Tunneling Electrical Connection to the Interior of Metal−Organic Frameworks. *J. Am. Chem. Soc.* **2015**, *137*, 8169−8175.
(20) Yaghi, O. M.; O'Keeffe, M.; Ockwig, N. W.; Chae, H. K.; Eddaoudi, M.; Kim, J. Reticular Synthesis and the Design of New Materials. *Nature* **2003**, *423*, 705−714.
(21) Arnold, W. A.; Winget, P.; Cramer, C. J. Reductive Dechlorination of 1,1,2,2-Tetrachloroethane. *Environ. Sci. Technol.* **2002**, *36*, 3536−3541.
(22) Maithreepala, R. A.; Doong, R.-a. Enhanced Dechlorination of Chlorinated Methanes and Ethenes by Chloride Green Rust in the Presence of Copper(II). *Environ. Sci. Technol.* **2005**, *39*, 4082−4090.
(23) Batten, S. R.; Neville, S. M.; Turner, D. R. *Coordination Polymers: Design, Analysis and Application*; Royal Society of Chemistry: Cambridge, UK, 2009.
(24) Spek, A. Single-Crystal Structure Validation with the Program Platon. *J. Appl. Crystallogr.* **2003**, *36*, 7−13.
(25) Spek, A. Structure Validation in Chemical Crystallography. *Acta Crystallogr., Sect. D: Biol. Crystallogr.* **2009**, *65*, 148−155.
(26) Ohmura, T.; Usuki, A.; Fukumori, K.; Ohta, T.; Ito, M.; Tatsumi, K. New Porphyrin-Based Metal−Organic Framework with High Porosity: 2-D Infinite 22.2-Å Square-Grid Coordination Network. *Inorg. Chem.* **2006**, *45*, 7988−7990.
(27) Brunschwig, B. S.; Creutz, C.; Sutin, N. Optical Transitions of Symmetrical Mixed-Valence Systems in the Class II-III Transition Regime. *Chem. Soc. Rev.* **2002**, *31*, 168−184.
(28) Zacher, D.; Shekhah, O.; Woll, C.; Fischer, R. A. Thin Films of Metal-Organic Frameworks. *Chem. Soc. Rev.* **2009**, *38*, 1418−1429.
(29) Stavila, V.; Volponi, J.; Katzenmeyer, A. M.; Dixon, M. C.; Allendorf, M. D. Kinetics and Mechanism of Metal-Organic Framework Thin Film Growth: Systematic Investigation of Hkust-1 Deposition on Qcm Electrodes. *Chem. Sci.* **2012**, *3*, 1531−1540.
(30) Rodenas, T.; Luz, I.; Prieto, G.; Seoane, B.; Miro, H.; Corma, A.; Kapteijn, F.; Llabrés i Xamena, F. X.; Gascon, J. Metal−Organic Framework Nanosheets in Polymer Composite Materials for Gas Separation. *Nat. Mater.* **2015**, *14*, 48−55.
(31) Hermosa, C.; Horrocks, B. R.; Martinez, J. I.; Liscio, F.; Gomez-Herrero, J.; Zamora, F. Mechanical and Optical Properties of Ultralarge Flakes of a Metal-Organic Framework with Molecular Thickness. *Chem. Sci.* **2015**, *6*, 2553−2558.
(32) Yu, Q.; Zhang, X.; Bian, H.; Liang, H.; Zhao, B.; Yan, S.; Liao, D. Ph-Dependent Cu(II) Coordination Polymers with Tetrazole-1-Acetic Acid: Synthesis, Crystal Structures, Epr and Magnetic Properties. *Cryst. Growth Des.* **2008**, *8*, 1140−1146.
(33) Kathalikkattil, A. C.; Bisht, K. K.; Aliaga-Alcalde, N.; Suresh, E. Synthesis, Magnetic Properties, and Structural Investigation of Mixed-Ligand Cu(II) Helical Coordination Polymers with an Amino Acid Backbone and N-Donor Propping: 1-D Helical, 2-D Hexagonal Net (Hcb), and 3-D Ins Topologies. *Cryst. Growth Des.* **2011**, *11*, 1631−1641.
(34) Agterberg, F. P. W.; Provó Kluit, H. A. J.; Driessen, W. L.; Oevering, H.; Buijs, W.; Lakin, M. T.; Spek, A. L.; Reedijk, J. Dinuclear Paddle-Wheel Copper(II) Carboxylates in the Catalytic Oxidation of Carboxylic Acids. Unusual Polymeric Chains Found in the Single-Crystal X-Ray Structures of [Tetrakis(M-1-Phenylcyclopropane-1-Carboxylato-O,O′)Bis(Ethanol-O)Dicopper(II)] and Catena-Poly-[[Bis(M-Diphenylacetato-O:O′)Dicopper](M3-Diphenylacetato-1-O:2-O′:1′-O′)(M3-Diphenylacetato-1-O:2-O′:2′-O′)]. *Inorg. Chem.* **1997**, *36*, 4321−4328.

DOI: 10.1021/acsami.6b03073
ACS Appl. Mater. Interfaces 2016, 8, 16154−16159